Structure
Article

Structure of a Bacteriophytochrome and Light-Stimulated Protomer Swapping with a Gene Repressor

Dom Bellini[1] and Miroslav Z. Papiz[1,*]
[1]Institute of Integrative Biology, Biosciences Building, University of Liverpool, Crown Street, Liverpool L69 7ZB, UK
*Correspondence: mpapiz@liverpool.ac.uk
http://dx.doi.org/10.1016/j.str.2012.06.002

SUMMARY

Phytochromes are photoreceptors in phototropic organisms that respond to light conditions by changing interactions between a response regulator and DNA. Bacterial phytochromes (BphPs) comprise an input photosensory core domain (PCD) and an output transducing domain (OTD). We report the structure of a BphP containing both PCD and the majority of its OTD, and demonstrate interaction with its cognate repressor. The OTD of *Rp*BphP1, from *Rhodopseudomonas palustris*, is composed of a PAS/PAC domain and, to our knowledge, a hitherto unrecognized two-helix output sensor (HOS) domain. Unlike canonical BphPs, it does not transmit phosphorelay signals but forms a complex with the transcriptional repressor *Rp*PpsR2 on photoconversion with far-red light. We show that HOS is essential for complex formation and that the anti-parallel dimer geometry is crucial in achieving HOS domain activation and protomer swapping under the control of light. These results provide insights into the steps taken by a two-component signaling system.

INTRODUCTION

Phytochromes are photoreceptors that respond to environmental light conditions and in so doing control a variety of photomorphogenic responses. They use a covalently bound linear tetrapyrrole molecule that reversibly photo-converts between the Pr (red) and Pfr (far-red) absorbing states. The light-dependent signal usually initiates phosphotransfer to a response regulator which, in turn, mediates differential expression of target genes. Phytochromes, initially discovered in plants, have now been described in many organisms such as cyanobacteria, fungi and bacteria (Bhoo et al., 2001; Davis et al., 1999; Giraud et al., 2002; Hughes et al., 1997; Lamparter et al., 2002). Bacteriophytochrome photoreceptors (BphPs) are bacterial homologs employing the chromophore biliverdin IXα (BV) and can be divided into two families; those with a dark stable Pr, and those with a dark stable Pfr state or as they are sometimes called bathy-BphPs (Giraud and Verméglio, 2008; Rottwinkel et al., 2010). The molecule can be divided into an input light-sensing N-terminal photo-sensory core domain (PCD) and a C-terminal output transducing domain (OTD). The PCD is composed of a Per/Arnt/Sim (PAS) domain followed by the cyclic di-GMP phosophodiesterase/adenyl cyclase/Fhla (GAF) domain and the phytochrome-associated (PHY) domain which is unique to phytochromes. The BV chromophore is found in the GAF domain and is covalently linked to a Cys residue at the N-terminus of the PAS domain. The C-terminal OTD shows more variability than the PCD because it depends on the particular response regulator it interacts with in the two-component regulatory system. The OTDs of canonical BphPs are homologues of the cytoplasmic domain of a histidine kinase (HK) (Bhoo et al., 2001; Davis et al., 1999; Rottwinkel et al., 2010) however other types of BphP exist with OTDs composed of a GGDEF/EAL domain (Kyndt et al., 2005; Tarutina et al., 2006) and are probably involved in second messenger signaling while the PAS/PAC domain variants are believed to bind directly to a repressor preventing its interaction with DNA (Giraud et al., 2002; Giraud and Verméglio, 2008). The OTDs composed of a PAS/PAC domain also have an ~90 amino acid sequence, at the C-terminus, which does not have a recognized homology with other structures (Giraud and Verméglio, 2008). Three-dimensional structures exist for the PCD (Essen et al., 2008; Yang et al., 2008) and the smaller chromophore binding domain (CBD) (Ulijasz et al., 2010; Wagner et al., 2005; Yang et al., 2007), but a structure of a complete BphP, containing both the PCD and associated OTD, has yet to be determined. In this study we describe the structure of the bathy-BphP *Rp*BphP1 from *Rhodopseudomonas palustris*, which plays a central role in the expression of a large cluster (>30) of photosynthetic genes (Giraud et al., 2002). The structure we present comprises a PCD and a major part of the OTD composed of PAS/PAC. Into this structure we have modeled, to our knowledge, the hitherto unassigned 90 amino acid C-terminal domain, which we name 2-Helix Output Sensor (HOS) domain, and we also show that it is essential for *Rp*BphP1 binding to the cognate repressor *Rp*PpsR2 on far-red light illumination. The structure gives an insight into a two-component regulatory system that involves only protein-protein interactions with a repressor molecule and not through the usual phosphor-relay mechanism. It is interesting to note that although *Rp*BphP1 is an atypical BphP, it shares a domain organization with the N-terminal part of plant phytochromes that possess two PAS domains following the PCD; the N-terminal domain organization is therefore PCD-PAS in both. *Rp*BphP1 may provide clues to plant phytochrome structures and also to the function of the PAS domains that are believed to be responsible for signal transduction.

RESULTS

*Rp*BphP1 Is an Antiparallel Dimer

The full length *Rp*BphP1 (~80 kDa) contains an unstable C-terminal domain (~10 kDa), which is usually lost by proteolysis within a week of sample preparation. Crystals grew only when the C-terminal domain was lost and the structure of the 70 kDa protein (*Rp*BphP1-N70) was determined by the Se-Met MAD/SAD method (Table 1; Table S1 available online). Other than by visualization of the structure, the size and position of the missing fragment was identified by molecular mass determination and an inability of the C-terminal His_6-tagged *Rp*BphP1 to bind to a Ni-affinity column implying the loss of a C terminus fragment. Four molecules were refined in the asymmetric unit containing residues ~8–635 with missing loops around ~451–458 within protomers B, C, and D. Analysis for oligomeric assemblies, with the program PISA (Krissinel and Henrick, 2007), points to two identical dimers formed between chains AD and BC. Dimers are antiparallel aligned protomers with a crossover angle ~135° and contacts made predominately between PAS/PAC (506–635) and PHY (320–505) domains in opposing protomers (Figure 1A). We are confident that they are molecular rather than crystal dimers based on size exclusion chromatography that confirms dimers in solution, in both the dark and on illumination with 760 nm light (Figure S1A); a high crystal solvent content (~66%), which provides good contrast between dimers; and a dimer interfacing surface area of 1909 $Å^3$, which is comparable to that of *Pa*BphP-PCD of *Pseudomonas aeruginosa* dimers, which is ~2081 $Å^3$. These dimers are strikingly different from canonical BphP dimers (Figure S5D), which possess a cytoplasmic HK domain at the OTD and show up in EM images as dimers formed from parallel protomers (Li et al., 2010). Unrelated HK structures also form parallel dimers and it has been proposed that this geometry is necessary for auto-phosphorylation (Casino et al., 2009; Marina et al., 2005; Yamada et al., 2009). The structure of the *Rp*BphP1-N70 protomer shows that PHY and PAS/PAC domains are isolated from one another by a slender ~30 Å helix *hI* but the antiparallel dimer geometry ensures that a large number of atomic contacts can be made between these domains, which can facilitate signal transmission. The overall structure of PCD in *Rp*BphP1-N70 is similar to that of *Pa*BphP-PCD (Yang et al., 2008) from *Pseudomonas aeruginosa*, both having disordered regions at PHY residues 443–459, leading to a short PHY helix *hG* (residues 460–463) which caps the BV binding pocket. A structural difference is found in *Rp*BphP1-N70 at residues 126–131 which are stretched due to a four residue deletion that shortens helix *hA* to 132–143 (Figures S2A and S2B). This is significant because helices *hA* and *hE* have been implicated in signal transduction (Ulijasz et al., 2010; Yang et al., 2008). Topologically there are obvious similarities between the PHY and PAS/PAC domains, which are both formed by long helices (*hE* and *hI*) followed by a domain that has a PAS-like topology (Figure 1B). Formally helix *hE* is shared between GAF and PHY domains and *hI* between PHY and PAS/PAC but structurally it makes more sense to pair them as *hE*-PHY and *hI*-PAS/PAC. At the dimer interface the two helices *hI* make extensive Van der Waals contacts between residues 504–528 and are tethered by hydrogen bonds Thr510-Ala520, Gln523-Arg506, Gln523-R509 at both ends (Figure 2A). Other dimer interactions are the salt bridge Glu515-Arg613 and hydrogen bonds Asp609-Gln504 formed between *hI* and PAS/PAC domain and Met528-Asp427, His428-Gln523, Glu367-Gln523, Arg509-Glu367, Ser527-Asp427 hydrogen bonds between *hI* and PHY

Table 1. Determination of Structure

Data Collection	Peak	Inflection	Remote Low	Remote High
X-ray source	DLS I03			DLS I03
Space group	$P2_1$			$P2_1$
Cell dimensions				
a, *b*, *c* (Å)	102.66			102.94
	143.00			146.86
	139.51			139.55
α, β, γ (°)	90.00			90.00
	101.71			101.17
	90.00			90.00
Wavelength (Å)	0.97911	0.97949	0.98244	0.97000
Resolution (Å)	66.5–3.4	61.9–3.4	64.4–3.4	73.4–2.9
	(3.5–3.4)[a]	(3.5–3.4)[a]	(3.5–3.4)[a]	(3.0–2.9)[a]
Rsym (%)	7.4 (27.3)	7.9 (31.5)	8.6 (38.7)	6.3 (28.8)
I / σ	11.9 (2.3)	11.9 (2.3)	11.1 (2.1)	9.2 (2.8)
Data completeness (%)	99.2 (96.5)	99.0 (97.8)	99.3 (98.4)	97.9 (96.5)
Multiplicity of reflections	6.8 (6.6)	6.5 (6.7)	6.7 (6.9)	3.4 (3.1)
Refinement Statistics				
Resolution range (Å)	15–2.9			
Number of reflections	83,855			
Number of atoms	19,771			
R-factor/ R-free (%)	19.8 / 24.4			
Mean atomic B-factors ($Å^2$)	72.4			
Coord error on R-free (Å)	0.35			
Bond R.m.s (Å)	0.015			
Angle R.m.s (°)	2.17			
Chiral volume R.m.s ($Å^3$)	0.10			
Core Ramachandran region (%)	76.7[b]			
Refined chains	A(8–635), B(8–451, 458–634), C(8–452, 457–633), D(8–443, 457–635)			
Refined Hetero molecules	4 Biliverdin IXα and 320 H_2O			

See also Table S1 and Figure S6.
[a]Values in parentheses are for highest resolution shell.
[b]A typical value, at a resolution of 2.9 Å, is 68.7%, PROCHECK (Laskowski et al., 1993).

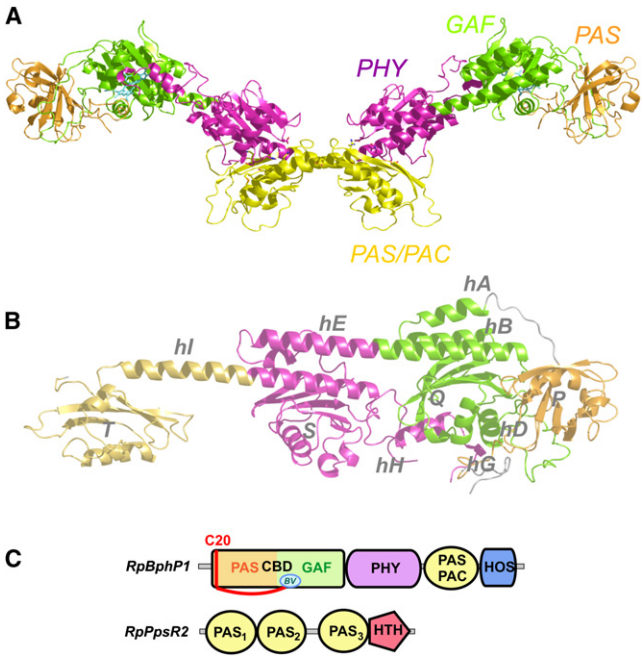

Figure 1. Structure of the *Rp*BphP1-N70 Dimer

(A) Structure of the dimer colored by domain: PAS, orange; GAF, green; PHY (phytochrome-associated), magenta; PAS/PAC (or PAS/S2-box), yellow; Biliverdin IXα, cyan.

(B) A single protomer rotated ~90° relative to (A) shows domain organization with helices discussed in the text marked *hA* to *hI*. The core PAS β strand topology is (*e2-e1-e5-e4-e3*) with α helices between *e2* and *e3*. This forms the core of a repeated motif marked P, Q, S, and T in domains PAS, GAF, PHY, and PAS/PAC.

(C) Domain organization of *Rp*BphP1 and *Rp*PpsR2. The chromophore binding domain (CBD) with biliverdin IXα (BV) located in the GAF domain covalently linked to PAS-Cys20. Domains are colored as in (A) and (B) with the HOS domain colored blue. *Rp*PpsR2 is composed of three PAS domains (yellow) followed by the DNA binding HTH domain colored purple.

See also Figures S1, S2, and S5.

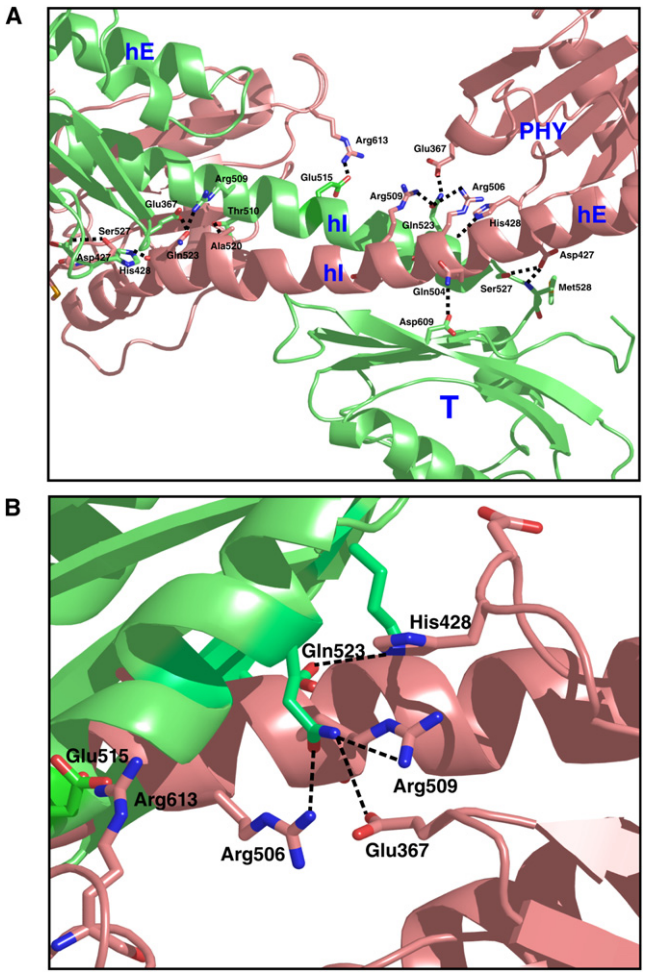

Figure 2. Dimerization Interface of *Rp*BphP1-N70

Protomers are colored green and salmon.

(A) dimer hydrogen(H)-bonding network is formed between *hI* helices and between the PAS/PAC and helix *hI*.

(B) amino acid Gln523 is positioned near the C-terminal of *hI* and forms several H-bonds with residues Glu367, His428, Arg506, and Arg509, locking together PAS/PAC and PHY domains of opposing protomers.

domain. The residue Gln523 is important as it makes several hydrogen bonds between protomers stabilizing *hI* with each other and the PHY domain (Figure 2B). This rather surprising antiparallel geometry probably arises from a very different structural requirement for binding to *Rp*PpsR2 rather than phosphotransfer. The structure also raises the interesting possibility that BphPs, with different OTD domains, may also have atypical dimer organizations.

HOS Domain Structure

We will show that the C-terminus (635–730) is required for binding to *Rp*PpsR2. Unfortunately most sequence homology search programs cannot identify homologous domains for the fragment (Giraud et al., 2002; Giraud and Verméglio, 2008). Although the fragment is easily degraded, it is by no means disordered and secondary structure predictions point to two long α-helical segments. We used the pair-wise Hidden Markov Model search program HHPred (Söding, 2005), which has superior sensitivity to homologous structures with low sequence identity. A high similarity was found between the C-terminal fragment and Dhp dimerization domains of cytoplasmic HK, composed of a helix-loop-helix motif (Tables S2A and S2B). The low sequence identity (~10%) and missing His residue, that renders it incapable of phosphorylation (Giraud et al., 2002), suggests that it is only a distant relative of Dhp. The highest alignment score is with ThkA (Yamada et al., 2009), which also has a PAS domain preceding Dhp. We propose that the OTD of *Rp*BphP1 evolved from PAS/PAC containing cytoplasmic HK domain (PAS/PAC-Dhp-KD) and then followed a deletion of the kinase domain resulting in the present OTD composed of PAS/PAC-Dhp. Because the Dhp-like domain in *Rp*BphP1 is sufficiently dissimilar in sequence and function to other Dhp domains, we propose the name 2-helix output sensor (HOS) domain. To obtain a full length model of *Rp*BphP1, HOS was remodelled (Sali and Blundell, 1993) to the correct sequence and docked (Ritchie et al., 2008) into *Rp*BphP1-N70 by an exhaustive geometry search and energy minimization. The procedure was essentially a six-dimensional rigid body search

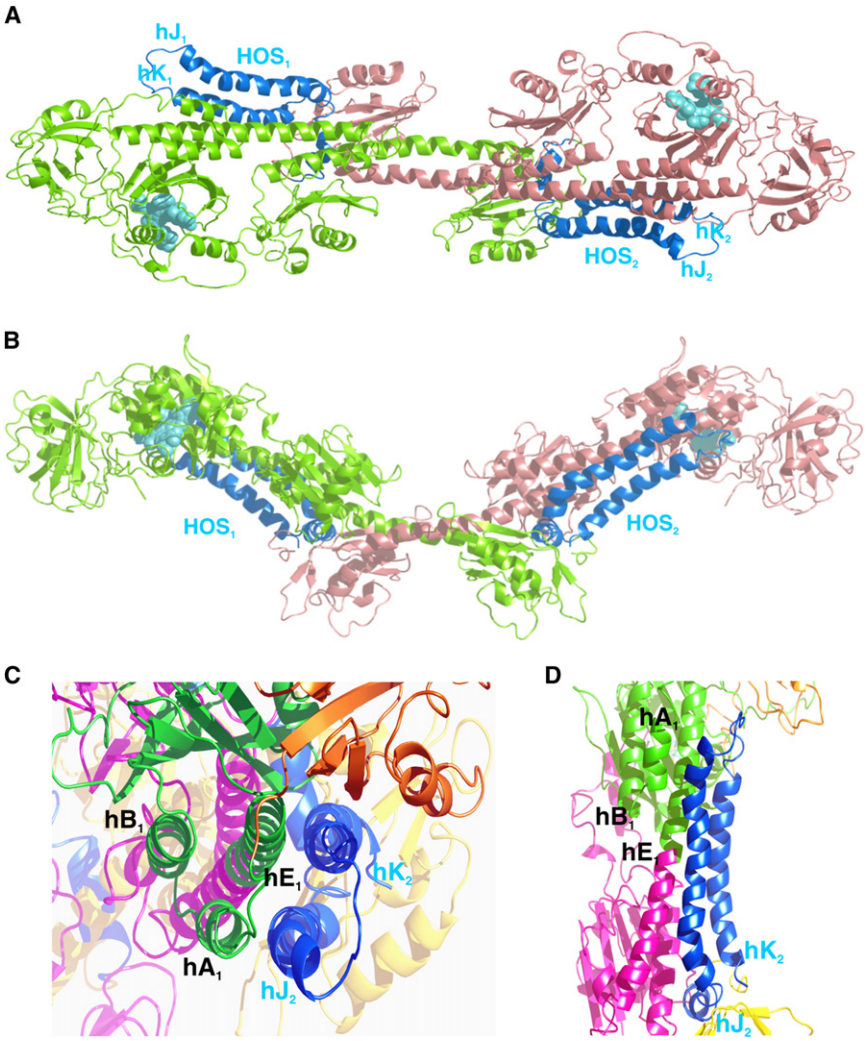

Figure 3. View of *Rp*BphP1 Dimer

(A and B) Protomers determined by X-ray diffraction are green and salmon, the modeled HOS domains in blue and BV cyan: top view (A), front view (B).

(C) and (D) are close views of the HOS region colored by domain as for Figure 1; looking down the four-helix heterodimer hA_1E_1-hJ_2K_2 formed by protomer 1 and HOS domain of protomer 2 (C) and from the front (D).

See also Tables S2 and S3 and Figure S4.

The BV Binding Site and the Photoconversion Mechanism

Progress has been made on determining the photoconversion mechanism and signal transduction in BphPs (Ulijasz et al., 2010; Wagner et al., 2008; Yang et al., 2009) and it has been proposed that, during photoconversion, BV undergoes a "flip and rotation" conformation change initiated by twisting of the pyrrole ring backbone (Yang et al., 2011) (Figure 4E). Photoconversion is therefore a complex process and the Pfr and Pr UV/visible absorption spectra characterize the start and end states only (Figure 4A). Because crystals are grown in the dark it is reasonable to assume that the *Rp*BphP1-N70 structure is of the Pfr state, and because dark spectra of *Rp*BphP1-N70 and *Rp*BphP1 are identical (Figures 4A and 4B), the overall structure probably also resembles *Rp*BphP1. There are differences in dark reversion times, from Pr to Pfr, for *Rp*BphP1 and *Rp*BphP1-N70. A dark reversion half-life of ~50 min is found for *Rp*BphP1 but is significantly faster (~3 min) for *Rp*BphP1-N70 and a Pr spectrum cannot be fully captured (Figure 4B). Interestingly, dark reversion kinetics of canonical BphP PCDs and their full length constructs are identical while truncated CBD constructs exhibit reduced photoconversion as judged by their spectra (Wagner et al., 2005; Yang et al., 2007, 2009), indicating that the PHY domain is important for stabilizing the conformation responsible for the Pr spectrum, while the spectrum of *Rp*BphP1-N70 is aberrant despite a larger structure containing both PCD and PAS/PAC. For the canonical structure *Pa*BphP-PCD (Yang et al., 2008) it has been proposed that the Pr state is stabilized when the BV pocket is capped by the PHY loop (453–459) with particular contributions from Arg453 and Ser459; Arg453 hydrogen bonds to Asp194, which then hydrogen bonds to the nitrogen atom in the D pyrrole and Ser459. In *Rp*BphP1-N70 this Arg is now Asp462 and is rotated away from the pocket so does not contribute to hydrogen bonding. Stabilization of the Pr conformation only occurs when the HOS domain is present. Variability in dark reversion kinetics is an interesting subject that may relate to light intensity sensing requirements within species and very fast (seconds) reversions have been reported

(rotation and translation) that docked HOS into *Rp*BphP1-N70, producing negligible changes in *Rp*BphP1-N70 and HOS conformation. The top three docking solutions deviated from one another by an RMS of ~3.6 Å. The resulting complete *Rp*BphP1 dimer has lower solvation energy, more hydrogen bond contacts, larger dimer dissociation energy, and a doubling of interfacing surface area (4325 Å) in comparison to *Rp*BphP1-N70 dimers (Table S3). Dhp domains normally form four-helix homodimeric bundles but HOS helices *hJ* and *hK* are too far from one another and instead take part in heterodimeric four-helix bundles with helices *hA* and *hE* (Figures 3A–3D). HOS helices *hJ* and *hK* interact with helices *hA* and *hE* at the beginning and the end of the GAF domain placing HOS at the heart of CBD and close to BV. As previously noted, helix *hA* is shortened in comparison to other PCD and CBD structures, allowing it to accommodate the formation of a *hAEJK* bundle, which requires only a short α-helix at this position. The interactions are further assisted by complementary shapes and electrostatic charges in the GAF/PHY and HOS surfaces (Figure S4). The modeling is a rigid body procedure, but in the real structure, additional conformational changes may also optimize the fit of HOS to *Rp*BphP1-N70.

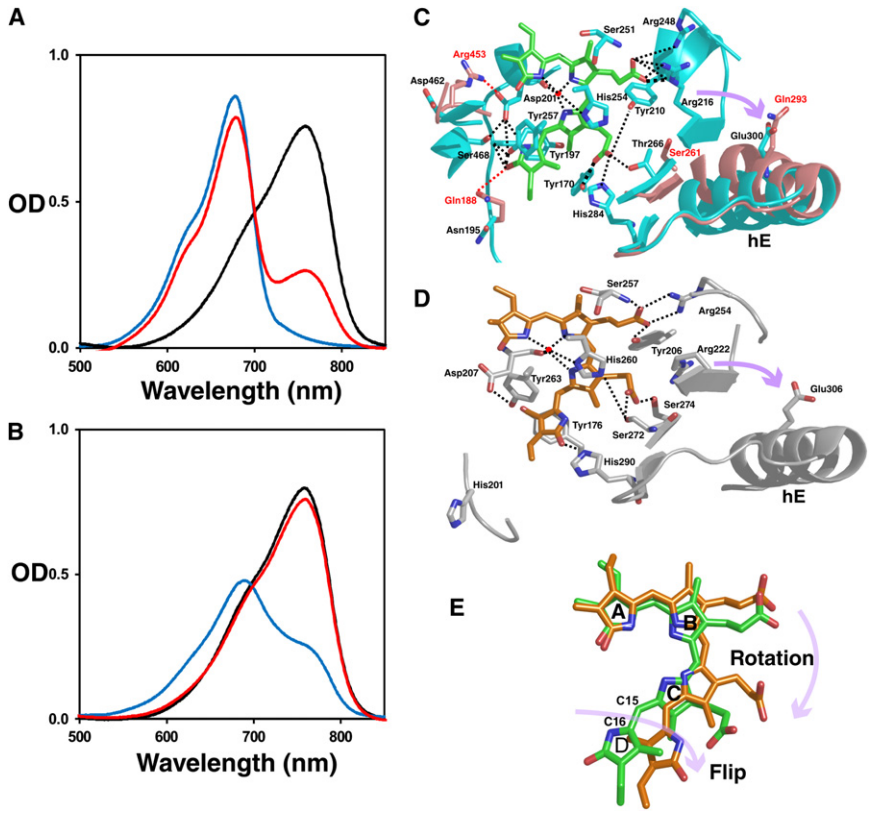

Figure 4. The Red/Far-Red UV/Visible Spectra and BV Binding Pocket

(A and B) *Rp*BphP1 (A) and *Rp*BphP1-N70 (B) showing the dark Pfr state centered on 760 nm (black), Pr state (blue) centered on 680 nm and the dark reversion spectrum (red) taken 30 min after photoconversion. Because of rapid dark reversion in *Rp*BphP1-N70 it is difficult to capture a pure Pr.

(C) The BV H-bonding network for *Rp*BphP1-N70 (black and cyan) and the *Pa*BphP-PCD domain from *Pseudomonas aeruginosa* (3C2W, red and salmon) both are in the Pfr state, for clarity only changes in *Pa*BphP-PCD that differ to *Rp*BphP1-N70 are shown.

(D) The Pr H-bonding network of *Dr*BphP-CBD (1ZTU) from *Deinococcus radiodurans*. NMR measurements on the GAF domain of *SyB*-Cph1 (Ulijasz et al., 2010) indicate a large movement, during photoconversion, of Arg101 from the propionate on ring B to Gln185 on helix *hE*. The equivalent residues are Arg216/Glu300, Arg209/Gln283 and Arg222/Glu306 in *Rp*BphP-N70, *Pa*BphP-PCD, and *Dr*BphP-CBD, respectively. Arrows indicate direction of movement of Arg.

(E) BV "flip and rotation" conformation change on photoconversion, Pfr (green) and Pr (orange). "Flip" is isomerization around C_{15} = C_{16} and "rotation" around an axis normal to the A pyrrole PDB ID 3G6O (Yang et al., 2009).

for some cyanobacteriochrome domains (Chen et al., 2012). The differences in stability may originate at the dimer interface, which is mostly intact in *Pa*BphP-PCD due to parallel protomer alignment (Yang et al., 2008) but is disrupted in *Rp*BphP1-N70 because of the missing HOS domains. In canonical BphPs spectral aberrations, such as quenching, can only be observed for the shorter CBD constructs in which the dimer interfacing helix *hE* is truncated by ~20 amino acids (Wagner et al., 2005; Yang et al., 2007). In *Rp*BphP1-N70 the loss of HOS helices *hJ* and *hK* destroys the four-helix bundle (*h*A-*h*E-*h*J-*h*K), which may affect Pr stability and the corresponding spectrum.

An alternative explanation of fast dark reversion kinetics may be disruption to the BV hydrogen bonding network; however, comparison of structures *Pa*BphP-PCD and *Rp*BphP1-N70 does not support this. The BV hydrogen bonding network of *Pa*BphP-PCD is rearranged to accommodate the "flip and rotation" motion of BV during photoconversion and analysis of *Rp*BphP1-N70 shows it to be similar in its H-bonding organization (Figures 4C and 4D). Hydrogen bonding in *Rp*BphP1-N70 BV pocket can be grouped into four distinguished clusters of interactions: (1) pyrrole nitrogen interactions with a water molecule, Asp201 carbonyl, and His254; (2) anchoring of the ring B propionate by Arg248 and Arg216; (3) anchoring of the ring C propionate by Tyr210, Thr248, and His248; and (4) anchoring of the ring D carbonyl by Asp201, Tyr257, and Ser468. In *Pa*BphP-PCD additional H-bonds, between BV and residues Arg453 and Gln188, provide further stability to the Pfr conformation, while the equivalent residues in *Rp*BphP1-N70 are Asp462 and Asn195 and do not H-bonds with BV. Mutations R453A and Q188L, in *Pa*BphP-PCD, slow down dark reversion times rather than increasing them suggesting that these differences are not the cause rapid dark reversion in *Rp*BphP1-N70. A mutation of residue Ser261 in *Pa*BphP-PCD does produce rapid dark reversion times (Yang et al., 2009), presumably because this residue stabilizes the Pr state as observed for *Dr*BphP-CBD-Pr (Figure 4D). In the structure of *Rp*BphP1-N70 the equivalent residue is the non H-bonding Val268 which, despite this, does not result in fast dark reversion times in the full length *Rp*BphP1 and it seems that the nearby Thr266 provides sufficient H-bonding constraints to the C ring propionate. The only other significant difference is that helix *hE*, in *Rp*BphP1-N70, is displaced away from the BV pocket by ~3 Å, which may be caused by the absence of the HOS domain. Helix *hE* is adjacent to β strand e4, which contains Thr266 and Val268, and the displacement of *hE* may provide the freedom for these residues to move away from BV during photoconversion destabilizing the Pr state. Disruption of the neighboring β strand e3 has been reported in the NMR Pr and Pfr structures of the GAF domain belonging to *SyB*-Cph1 of *Synechococcus* OSB′. These NMR structures show a large movement of Arg101 from the propionate on ring B to Gln185 on *hE* during photoconversion (Ulijasz et al., 2010). The equivalent residues in *Rp*BphP1-N70 are Arg216 and Glu300 on *hE* (Figure 4C) and the displaced helix *hE* may prevent the formation of an efficient salt bridge, which also may cause the destabilization of Pr. A *caveat* concerning *SyB*-Cph1 is the different chromophore (phycocyanobilin) that is used and a dark stable Pr rather than Pfr, but in other respects the bilin H-bonding networks are comparable. PCDs appear to

be conserved motifs in BphP and so the Arg to Gln/Glu motion, between the bilin and the signaling helix *hE*, may be a parsimonious solution to the mechanism of signal transduction that is used by all BphPs irrespective of the OTD. The importance of long helices has been recognized in other signaling proteins and a consensus 40 residue signaling S-helix motif has been proposed for signal transmission between modules in prokaryotic signaling proteins (Anantharaman et al., 2006).

Protomer Swapping in *Rp*BphP1 during Photoconversion

In *Rps. palustris* photosynthesis is activated by far-red light (Evans et al., 2005; Giraud et al., 2002) and it has been proposed that *Rp*BphP1 is the antirepressor of *Rp*PpsR2 (Braatsch et al., 2006, 2007; Giraud et al., 2002). Before investigating this interaction, we measured the behavior of *Rp*BphP1 dimers on illumination with 760 nm light. Size exclusion chromatography measurements show that, in the dark and on illumination with 760 nm light, only *Rp*BphP1 dimers are present (i.e., no monomeric forms were detected), with an apparent molecular mass of ~225 kDa (Figure S1A). Elongated molecular shapes explain a larger than expected molecular mass and values of 250 kDa are common for other BphPs (Wagner et al., 2007). The most surprising results were observed during light induced Ni-affinity chromatography binding experiments. The purity of tagged and untagged *Rp*BphP1 was high in these experiments as both were overexpressed by *Escherichia coli*, from tagged and untagged plasmids, at 40 mg per liter and Ni-affinity or ion-exchange chromatography followed by gel filtration resulted in SDS-PAGE gels showing a single band for *Rp*BphP1. A dark incubated sample, containing an excess of untagged *Rp*BphP1 mixed with N-terminal His_6-tagged *Rp*BphP1, elutes at an imidazole concentration of ~10 mM for untagged and ~430 mM for His_6-tagged protein (Figures S3A and S3B). After incubation with 760 nm light, elution data show a reduction of the untagged peak and a gain in the His_6-tagged peak observed as a double profile at 365 and 430 mM (Figures 5A–5C). This can be interpreted as monomer swapping between tagged and untagged dimers making hetero-tagged dimers eluting at 365 mM due to one His-tagged protomer in the heterodimer. The fact that some of the 430 mM peak is still present points to some doubly His-tagged molecules failing to photo-convert to Pr because of high sample absorption at 760 nm and a relatively long optical path. When the 365- to 430-mM eluted peaks (P2 and P3) are reloaded onto a Ni-affinity column, after further illumination with 760 nm light, it is observed that untagged homodimers are formed from a sample containing only singly and doubly His-tagged dimers (Figure S3D). Similar experiments with untagged *Rp*BphP1-N70 and His_6-*Rp*BphP1 protein showed that hetero-tagged dimers do not form on illumination with light. *Rp*BphP1-N70 was obtained from a previously purified full length C-terminal His-tagged *Rp*BphP1 which was allowed to degrade so that it lost its ability to bind to a Ni-affinity column. This sample was also used for the crystallization of *Rp*BphP1-N70. The resulting structure establishes that *Rp*BphP1-N70 is a fragment containing residues 8–635. These two results establish that the missing HOS domain is (635–730). The inability of *Rp*BphP1-N70 to protomer swap with a full length N-terminal tagged *Rp*Bph1, on illumination, strongly suggests that HOS plays an active role in protomer swapping. Taken together these experiments show that: (a) far-red light and therefore the Pr conformation is essential for protomer swapping, (b) the C-terminal HOS (635–730) domain is required to stabilize the Pr state and may also play an active role in the exchange mechanism, and (c) tetramers or free monomers are absent, or present in very low amounts, since dark and 760 nm light illumination gel chromatography results superimpose (Figure S1A). The results suggest that hetero-tagged dimers are formed on photoconversion through a rapid exchange of protomers (or swapping) between dimers. Whether it proceeds by the formation of tetramers or by dissociation into monomers is to be determined, however the absence of either, in gel filtration chromatography experiments, indicates that this must be a quick and efficient process.

*Rp*BphP1-*Rp*PpsR2 Complexes Are Formed after Photoconversion

In most phototropic bacteria photosynthesis is optimal at low oxygen levels or microaerobic conditions. Binding of the gene repressor PpsR2 to DNA is controlled, in *Rb. capsulatus* and *Rb. sphaeroides*, by the formation of intra disulfide bridges (Masuda and Bauer, 2002; Masuda et al., 2002). However *Rp*PpsR2 contains a sole cysteine at position 439 in the predicted helix-turn-helix (HTH) DNA-binding domain and can only form inter protomer disulfide bonds, as revealed by combining the results from SDS PAGE gels (Figure S5A) and size exclusion chromatography (Figure S1B); both oxidized and reduced forms are dimeric despite a broken disulfide bond in the reduced form. It is known that in *Rps. palustris* strain CGA009 (Braatsch et al., 2006) low cellular oxygen is one of the important factors in removing the repression of gene transcription by PpsR2 and for this reason experiments were carried out in the presence of dithiothreitol. *Rp*PpsR2 in other strains of *Rps. palustris* do not possess Cys residues or when they do they are at unconserved positions, which indicates that PpsR2 in these strains may not be redox sensitive and respond only to light through interactions with *Rp*BphP1. To investigate this Ni-affinity chromatography was performed with 760 nm illuminated samples, containing N-terminal His_6-tagged *Rp*PpsR2 and an excess of untagged *Rp*BphP1 or untagged *Rp*BphP1-N70, and revealed the formation of a complex between *Rp*PpsR2 and *Rp*BphP1 but not with RpBphP1-N70 (Figures 5E–5G); because elution was monitored at two wavelengths, 400 nm and 280 nm, complexes composed of both proteins or dimers containing only *Rp*PpsR2 could be differentiated. The experiments clearly show that an untagged *Rp*BphP1 is only retained by the Ni-affinity column when in complex with *Rp*PpsR2 and it can be calculated from absorption to be in the molar ratio of 1. The fraction bound to the Ni-affinity column also shows the presence of both *Rp*BphP1 and *Rp*PpsR2 in SDS-PAGE electrophoresis gels (Figure S5C). The 400nm wavelength is sensitive to the presence of even the smallest amount of complex and the complete absence of *Rp*PpsR2-*Rp*BphP1-N70 indicates that the shortened lifetime of the Pr state cannot be the only reason for this and points to an essential role played by HOS in complex formation. It is probable that the HOS domain is tightly bound within an *h*A-*h*E-*h*J-*h*K helix bundle in the dark but less tightly bound or labile in the Pr state making it available for interaction with *Rp*PpsR2. This

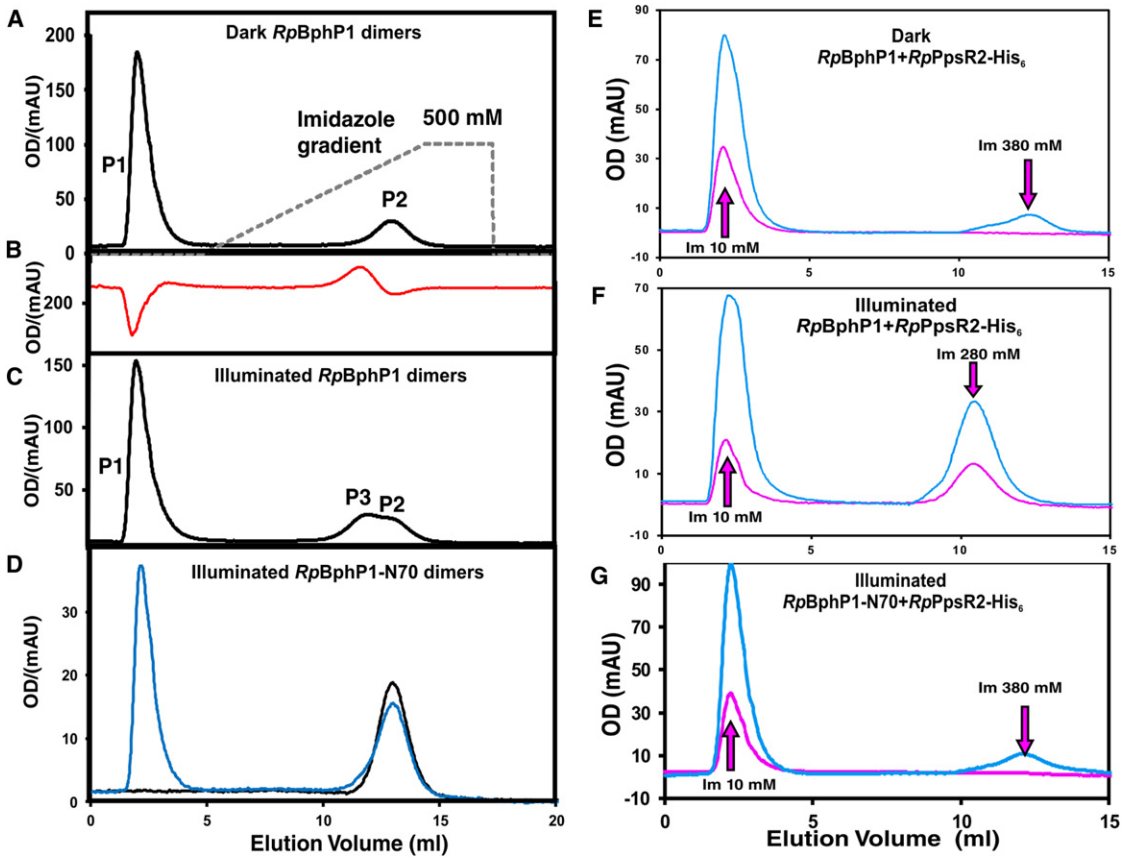

Figure 5. Protomer Swapping, as Observed on an Ni-Affinity Column, Monitored at the BV Absorption Wavelength 400 nm

(A–C) Tagged and untagged protein was mixed in the ratio ~1:4. In 760 nm light protomer swapping is seen for *Rp*BphP1 but not for *Rp*BphP1-N70 dimers; (A) in the dark untagged *Rp*BphP1 dimers elute at 10 mM Imidazole (peak area *P1* = 181) and His_6-*Rp*BphP1 at 430 mM (*P2* = 39); (C) after illumination with 760 nm light the 10 mM peak is reduced and a new peak *P3*, composed of a heterodimer His_6-RpBphP1/RpBphP1, elutes at 365 mM (*P1* = 161, *P2*+*P3* = 57); (B) is the difference of (C)−(A) showing the increase and decrease of peaks; (D) elution of untagged *Rp*BphP1-N70 dimers + His_6-*Rp*BphP1 dimers (blue), after 760 nm illumination, shows no protomer swapping between dimers despite the presence of a full length protein *Rp*BphP1. For comparison the elution of only His_6-*Rp*BphP1 is shown in black. Elution in (A)–(D) were measured at the BV absorption wavelength of 400 nm.

(E–G) Elution profiles of untagged *Rp*BphP1 or untagged *Rp*BphP1-N70 mixed with His_6-*Rp*PpsR2 (~4:1), monitored at 280 nm and corrected for imidazole absorption (blue) and at 400 nm (magenta); in the dark His_6-*Rp*PpsR2 elutes at 380 mM imidazole and untagged-*Rp*BphP1 at 10 mM (E); after illuminating with 760 nm light *Rp*BphP1/His_6-*Rp*PpsR2 complexes elute at ~280 mM and is indicated by the presence of 400 nm absorption and an increase in 280 nm absorption (F); a similar experiment with *Rp*BphP1-N70 in light shows no complex formation, which indicates that HOS is essential for complex formation (G). Molar ratios of complex formation were calculated from integrated peak absorption values in spectra (E) and (F) at wavelengths 400 nm and 280 nm, using $\varepsilon(280nm)_{RpBphP1}$ = 59,800; ε $(280nm)_{RpPpsR2}$ = 39,200; and ε $(400nm)_{RpBphP1}$ = 26,900, and are as follows OD(*Rp*BphP1(400))/OD(*Rp*PpsR2(280)) and OD(*Rp*BphP1(280))/OD(*Rp*PpsR2(280)) are 1.14 and 0.80, respectively.

See also Figures S3 and S5.

correlates with a propensity for HOS proteolysis when strict darkness is not maintained during sample preparation.

DISCUSSION

Anti-Repressor Mechanism

To our knowledge, this is a report of the first structure of a BphP including the CBD, PHY, and OTD domains. The structures of canonical PCD and CBD fragments, and EM images of full length BphPs, all belonging to the HK family, indicate that the *Rp*BphP1 dimer geometry presented here is radically different (Figure S5D) and points to the OTD in *Rp*BphP1 exerting a major influence on dimer formation. Different OTDs can provide new functionalities to BphPs and now it is also clear that new oligomer geometries arise that can make use of photoconversion changes in novel ways. Domain swapping has been well documented (Bennett et al., 1995) but protomer swapping, as observed between *Rp*BphP1 dimers and under the control of light, to our knowledge has not been observed before. This could also be the mechanism utilized for the formation of the *Rp*BphP1-*Rp*PpsR2 hetero-complexes, as is observed by Ni-affinity chromatography; however to experimentally establish the nature of this hetero-interaction (i.e., to estimate the molecular ratios in the hetero-complex) has proved to be technically challenging because of a combination of effects such as low solubility of *Rp*PpsR2, dark reversion of *Rp*BphP1, and overlapping gel filtration peaks. Although indirect evidence exists in vivo suggesting that *Rp*BphP1 may interact with the DNA-binding repressor

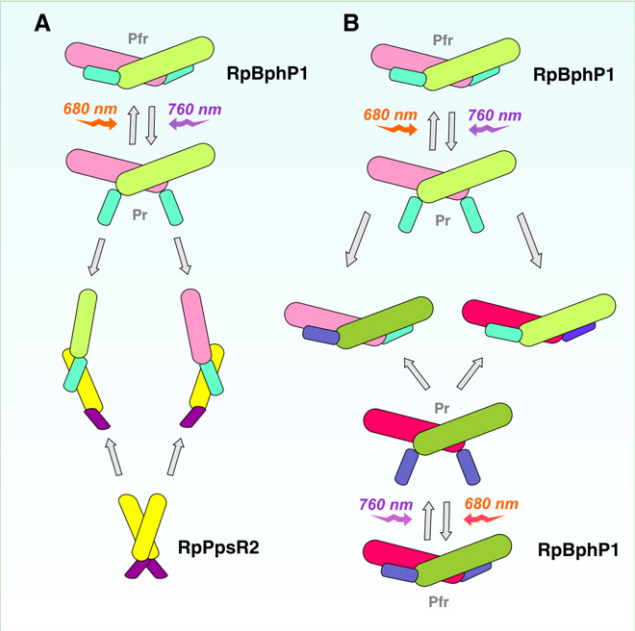

Figure 6. Protomer Swapping Stimulated by 760 nm Light
Swapping between (A) *Rp*BphP1 and *Rp*PpsR2 dimers to form *Rp*PpsR2-*Rp*PpsR2 complexes and (B) between two *Rp*Bph1 dimers. The HOS domains (cyan and blue) are made active when *Rp*BphP1 is in the Pr state enabling the subunits of one dimer to swap with the subunits of another dimer. In (B, center), protomer swapping continues until it is halted in the absence of light and dark reversion to Pfr.
See also Figures S3 and S5.

*Rp*PpsR2 (Braatsch et al., 2006, 2007; Evans et al., 2005; Giraud et al., 2002), our results directly show the interaction between a bacteriophytochrome and its cognate repressor and provide a plausible explanation of how *Rp*BphP1 could disrupt *Rp*PpsR2 transcription repression by the formation of heterodimers. It is interesting to note that if *Rp*BphP1-*Rp*PpsR2 complexes are formed by protomer swapping, as is observed in the case of *Rp*BphP1 with itself, the reduced form of *Rp*PpsR2 allows this because the absence of an inter protomer disulfide bond makes protomers separable. Thus a hetero-complex formation through protomer swapping would provide a mechanism accounting for *Rp*PpsR2 ability to respond to both light and redox environmental changes (Figure 6A). The fact that cysteine residues are absent in PpsR2 of other *Rps palustris* strains suggests that PpsR2 may not have redox sensing capabilities in all strains and for those cases they are probably only under the control of far-red light.

Role of OTD in Complex Formation

PAS domains are often involved in hetero-complex formation (Taylor and Zhulin, 1999) and it is likely that both PAS/PAC and HOS domains make atomic contacts with *Rp*PpsR2. Modeling of *Rp*PpsR2 indicates the presence of a long helix that could also be the site of interaction with HOS helices (Figure S5B). An example of helices, adjacent to PAS domains, that transmit signals is the circadian clock *Drosophila* period protein (PER) which is a dimer composed of monomers made from a pair of PAS domains and protruding α helices that unlatch switching association of PER to its partner Timeless (King et al., 2011). We conclude that HOS is a labile domain designed to move between *Rp*BphP1 and *Rp*PpsR2 facilitating complex formation. The labile nature of HOS may also provide a degradation pathway for a more responsive light-sensing system. Degradation can be important for modulating light-sensing as has been observed in the plant phytochrome phyA which forms the conjugate phyA-ubiquitin for proteolysis by the 26S proteasome pathway removing it from the system (Clough and Vierstra, 1997).

Cell Signaling by Protein-Protein Interactions

Mechanisms in cell signaling usually include a wide range of interactions such as phosphorelay (pTyr, pSer, pHis), chemical second messengers (cGMP, cAMP, IP3), binding of factors to receptors, modification of proteins in the cascade by ubiquitination, or post-translational modification (e.g., glycosylation). In eukaryotes they often involve a complex cascade of transfers and other interactions before gene responses are modified, which makes the study of the complete process difficult. Less well studied signaling mechanisms are those by protein-protein interactions (Kim et al., 2002). These may be an important class of signaling protein as they represent a more direct mechanism of controlling transcription. On the simplest level the study of such mechanisms requires the sensor, transducer, output domains and the response regulator which binds to DNA. The system we present here has these components and therefore allows the study of signaling from the sensor event (light) through to changes in repressor behavior. The important feature of the mechanism is the modification of oligomeric interactions on far-red light. By activation of the OTD and specifically HOS, protomer swapping is induced between homodimers resulting in heterodimer complexes that inactivate *Rp*PpsR2. Response regulators usually bind to DNA as dimers or tetramers, and the disruption of these oligomeric forms could be a common mechanism of signal control in protein-protein disruption signaling.

Plant Phytochromes

Plant phytochromes contain two PAS domains between the PCD and the HK domain and share a 26% amino acid sequence identity with *Rp*BphP1 over the region covered by *Rp*BphP1-N70 (i.e., PCD-PAS/PAC). The partial OTD of *Rp*BphP1-N70 is a long helix *hI* followed by PAS/PAC and this is mirrored in the *hE*-PAS organization of the preceding PHY domain which has a PAS like domain at its core. This then appears to be a common repeating motif in phytochromes. A homology search with *hI*-PAS/PAC as the template pulls out the two *hX*-PAS signaling motifs in plant phytochromes phyA and phyB of *Arabidopsis thaliana*. This search also finds many hits in other signaling proteins other than BphPs and suggests it is a prevalent and important motif for signal transduction. It is interesting to speculate why this domain appears in tandem within *Rp*BphP1 while in plant phytochromes as three motifs *h*-PHY-*h*-PAS-*h*-PAS. One explanation could be that these multiple domains provide a mechanism for transmitting signals over longer distances by "daisy" chaining together these modules. The plant phytochromes and *Rp*BphP1 may have evolved from a common ancestral phytochrome composed of an OTD made of a PAS containing HK, with the overall phytochrome domain

organization PCD-PAS-Dhp-KD; the dimerization domain (Dhp) and kinase domain (KD) together making the canonical cytoplasmic histidine kinase domain. *Rp*BphP1 was then formed by deletion of KD to make PCD-PAS-Dhp and Dhp then evolved to HOS with a new function while the canonical plant phytochromes duplicated PAS to make PCD-PAS-PAS-Dhp-KD. *Rp*BphP1 could therefore be a model for investigating the N-terminal photosensory and signal tranducing domains of plant phytochromes and may be thought of as the "missing link" between bacterial and plant phytochromes. The gene *rpbph1* is a repaired gene rpa1537 with closest relationship to B3Q7C0 of *Rps. palustris* in strain TIE-1.

EXPERIMENTAL PROCEDURES

Cloning and Purification

The gene *rpa1537* encodes for the baceriophytochrome *Rp*BphP1 from *Rhodopseudomonas palustris* strain CGA009 and is frame shifted but is otherwise intact in other strains and has been shown to be functional when corrected and inserted into CGA009 (Braatsch et al., 2006, 2007). The corrected gene *rpbph1* was used in this work and has closest relationship to B3Q7C0 of *Rps. palustris* in strain TIE-1. The gene was designed in silico, to have an *NdeI* restriction site at the 5′ end and a HindIII site, a stop codon and a *XhoI* site, in this order, at the 3′ and was made by Genscript inserted in pUC57. Using the STRU-cloning protocol (Bellini et al., 2011), *bphP1* was sub-cloned into pET28a (using *NdeI* and HindIII sites), pET24a (using *NdeI* and HindIII sites) and pET24a (using *NdeI* and *XhoI* sites) to obtain expression constructs for N-terminal His_6-tagged, C-terminal His_6-tagged and untagged protein, respectively. Transformed *E.coli* BL21 (DE3) were induced with 0.02 mM IPTG and left growing overnight at 18°C. Se-Met protein was expressed by the metabolic inhibition method, using 1L of LB medium enriched with 50 mg of leucine, isoleucine and valine, 100 mg of lysine, phenylalanine, and threonine and 80 mg of Se-Met, all added 15 min before IPTG induction. Harvested cell pellets were re-suspended in suitable chromatography buffers containing 10 mM Bilivirdin IXα (Frontier Scientific, Inc.) and protease inhibitor tablets (Roche) and French pressed to disrupt cells. DNase I (10 μg/ml) was added followed by Triton X-100 to a final concentration of 0.5% to disrupt weak hydrophobic interaction between *Rp*BphP1 and most probably the cell membrane. Protein was purified on His-Trap HP or HiTrap QFF 5 ml columns (GE Healthcare) in the case of His_6-tagged or untagged protein, respectively, and gel filtered using a HiLoad 26/60 Superdex200 column (GE Healthcare) in 5 mM TrisHCl pH 8 and 10 mM NaCl. The plasmid pETPSPL (pET28a) containing the *Rhodospeudomonas palustris* gene *ppsR2* was kindly provided by Shinji Masuda (Tokyo Institute of Technology) and Tom Beatty (University of British Columbia). The protein N-His_6-*Rp*PpsR2 (pET28a) was expressed in *E. coli* BL21 (DE3) and induced with 0.5 mM IPTG overnight at 18°C. It was purified on a His-Trap HP column followed by gel filtration and stored in a reduced environment of final buffer 20 mM Tris-HCl pH 8, 300 mM NaCl, and 5 mM dithiothreitol (DTT).

UV/Visible Spectroscopy

UV/Visible spectra were recorded at room temperature on a Perkin Elmer Lambda 35 UV/VIS spectrometer. Spectra were recorded either in the dark or after illuminating the sample with light passed through an interference filter centered on 760 (±10) nm (Knight Optical, Ltd.). The filter achieved ~100% photoconversion from Pfr to Pr. Photoconversion measurements were carried out in UVette cells (Eppendorf), which hold 50–100 μl sample volumes, have 10 mm optical paths for UV/Visible spectrum measurements and a 2 mm optical path, at right angles, to induce photoconversion.

Crystallization and Data Collection

Untagged *Rp*BphP1-N70 was purified by collecting the flow-through from Ni(II) affinity chromatography using a previously purified C-terminal His_6-tagged *Rp*BphP1 sample that was reloaded onto the Ni(II) affinity column only after SDS-PAGE gels showed an almost complete degradation of the C-terminal HOS fragment, which usually occurred at a concentration of 20 mg/ml and a temperature of 4°C in about 1 to 2 weeks. *Rp*BphP1-N70 was crystallized in a 96 well sitting drop format using a Screemaker 96+8 crystallization robot (Gilson). The final condition was optimized to be 4% poly-γ-glutamic acid polymer (PGA), Molecular Dimensions Ltd, 0.4 M Niacinamide, 200 mM KBr and 100 mM TrisHCl pH 8, at a protein concentration of 20 mg/ml at 20°C. Crystals grew as green thin plates (200 × 200 × 30 μm) and were viewed by passing white light through an interference filter (Knight Optical, Ltd.) centered at 500 (±20) nm, which is a BV none absorbing region, enabling crystals to be harvested and cryo-protected with 25% ethylene glycol. Diffraction data were collected with a Pilatus 6M-F detector at 100 K on the synchrotron beam line I03, Diamond Source Ltd. Images were indexed, integrated and scaled using Xia2, XDS (Kabsch, 2010), SCALA (Winn et al., 2011).

Structure Determination and Refinement

The crystal structure of Se-Met *Rp*BphP1-N70 was determined by Se-MAD/SAD phasing using CCP4 suite of programs (Winn et al., 2011). One crystal was used to measure Se-MAD data to a resolution of 3.4 Å at Se inflection, peak and low remote energies and a stronger SAD dataset was measured on another crystal at 2.9 Å resolution and high remote energies. The SAD dataset was used in phasing and also for structure refinement. The *Se* substructure was determined in SHELXD (Schneider and Sheldrick, 2002) which found 45 Se atoms with correlation coefficients 0.45/0.25 for strong/weak reflections. The program autoSHARP (Vonrhein et al., 2007) was used to augment Se sites to 52 and to calculate protein crystal phases to 3.0 Å (Table S1). The data in the range 3.4 to 3.0 Å was therefore primarily phased with SAD data from crystal 2. The experimentally phased map was improved by five cycles of solvent flattening and histogram matching using a solvent fraction 0.64. This gave a readily interpretable electron density map (Figure S6). The starting map was of sufficient quality to automatically build 80% of the atomic model using the program Buccaneer (Cowtan, 2006). Later maps were further improved, using DM and PARROT (Winn et al., 2011), by NCS averaging of the four molecular copies. The remaining structure was modeled in Coot 6.2 (Emsley and Cowtan, 2004) and refined with REFMAC5 (Murshudov et al., 2011) using loose NCS restraints and isotropic atomic temperature augmented with a TLS thermal model defined by each monomer. The structure was refined with the scale factor between X-ray and geometric parameters determined automatically by REFMAC5 and the final model was refined to R_{factor} 19.8% and R_{free} 24.4%, Table 1. The structure bond and angle geometry is 0.015 Å and 2.17°, respectively, and 76.7% of residues were calculated, by PROCHECK, to be in the 'core' favored Ramachandran region. This is better than the value of 68.7% predicted by PROCHECK for data at 2.9 Å resolution (Laskowski et al., 1993). The structure contains chain A (8–635), chain B (8–451, 458–634), chain C (8–452, 457–633), chain D (8–443, 457–635), 4 biliverdin IXα and 320 water molecules. PyMOL (Molecular Graphics System) and CCP4mg (Winn et al., 2011) were used to illustrate the structure. Superimposition and comparison of structures was made with the program RAPIDO (Mosca and Schneider, 2008).

Gel Filtration Analysis

Purified protein (200 μl of approximately 3 mg/ml) were loaded onto a Superose 12 10/300 GL (GE Healthcare) using an ÄKTA Explorer (GE Healthcare). For *Rp*BphP1 this was done either in the dark or quickly after illumination at 760 nm for 20 min. The column was calibrated using the high-molecular-weight calibration kit (GE Healthcare).

*Rp*BphP1 Monomer Swapping in Dimers by Ni(II) Affinity Chromatography

Purified N-terminal His-tag and untagged *Rp*BphP1 were mixed in a ratio ~1:4. Samples were either incubated in the dark or illuminated for 20 minutes at 760 nm to achieve a Pr state. Chromatography was carried out over a period of 10 min using a 1 ml His-Trap HP column and an ÄKTA Explorer. The elution profile was monitored at the high energy biliverdin absorption wavelength 400 nm which is also the isosbestic point of Pr/Pfr states.

Detection of *Rp*BphP1 Binding to *Rp*PpsR2 by Ni(II) Affinity Chromatography

Purified N-terminal His_6-tagged *Rp*PpsR2 and untagged *Rp*BphP1 were mixed in a ratio ~1:4 and applied to a Ni-affinity chromatography column as

above, after illumination. Elution spectra were monitored at 280 and 400 nm to differentiate peaks containing both His_6-*Rp*PpsR2 and *Rp*BphP1 or only His_6-*Rp*PpsR2 or *Rp*BphP1. Because *Rp*BphP1 is untagged it can only bind to the column when it is part of the complex His_6-*Rp*PpsR2-*Rp*BphP1.

Homology Search and Docking

An orthologous structure to the *Rp*BphP1 C-terminal fragment (635–730) was found (Tables S2A and S2B) using a Hidden Markov Model comparison program HHPred (Söding, 2005). The orthologous fragment was rebuilt to the correct *Rp*BphP1 amino acid sequence using Modeler 9.3 (Sali and Blundell, 1993) and docked to *Rp*BphP1-N70 with the program Hex 6.3 (Ritchie et al., 2008), which uses a rigid body geometry/energy search algorithm that samples several thousand orientations and fits each orientation by molecular mechanics energy minimization.

ACCESSION NUMBERS

The PDB accession number for the coordinates of the structure *Rp*BphP1-N70 reported in this paper is 4EHO.

SUPPLEMENTAL INFORMATION

Supplemental Information includes six figures and three tables and can be found with this article online at http://dx.doi.org/10.1016/j.str.2012.06.002.

ACKNOWLEDGMENTS

We would like to thank the Biotechnology and Biological Sciences Research Council (Grant BB/E002609/2) and the Science and Technology Facilities Council for supporting the work. The plasmid pETPSPL containing the *Rhodospeudomonas palustris* gene *ppsR2* was kindly provided by Shinji Masuda (Tokyo Institute of Technology) and Tom Beatty (University of British Columbia).

Received: January 20, 2012
Revised: May 19, 2012
Accepted: June 2, 2012
Published online: July 12, 2012

REFERENCES

Anantharaman, V., Balaji, S., and Aravind, L. (2006). The signaling helix: a common functional theme in diverse signaling proteins. Biol. Direct *1*, 25.

Bellini, D., Fordham-Skelton, A.P., and Papiz, M.Z. (2011). STRU-cloning: a fast, inexpensive and efficient cloning procedure applicable to both small scale and structural genomics size cloning. Mol. Biotechnol. *48*, 30–37.

Bennett, M.J., Schlunegger, M.P., and Eisenberg, D. (1995). 3D domain swapping: a mechanism for oligomer assembly. Protein Sci. *4*, 2455–2468.

Bhoo, S.H., Davis, S.J., Walker, J., Karniol, B., and Vierstra, R.D. (2001). Bacteriophytochromes are photochromic histidine kinases using a biliverdin chromophore. Nature *414*, 776–779.

Braatsch, S., Bernstein, J.R., Lessner, F., Morgan, J., Liao, J.C., Harwood, C.S., and Beatty, J.T. (2006). Rhodopseudomonas palustris CGA009 has two functional ppsR genes, each of which encodes a repressor of photosynthesis gene expression. Biochemistry *45*, 14441–14451.

Braatsch, S., Johnson, J.A., Noll, K., and Beatty, J.T. (2007). The O2-responsive repressor PpsR2 but not PpsR1 transduces a light signal sensed by the BphP1 phytochrome in Rhodopseudomonas palustris CGA009. FEMS Microbiol. Lett. *272*, 60–64.

Casino, P., Rubio, V., and Marina, A. (2009). Structural insight into partner specificity and phosphoryl transfer in two-component signal transduction. Cell *139*, 325–336.

Chen, Y., Zhang, J., Luo, J., Tu, J.M., Zeng, X.L., Xie, J., Zhou, M., Zhao, J.Q., Scheer, H., and Zhao, K.H. (2012). Photophysical diversity of two novel cyanobacteriochromes with phycocyanobilin chromophores: photochemistry and dark reversion kinetics. FEBS J. *279*, 40–54.

Clough, R.C., and Vierstra, R.D. (1997). Phytochrome degradation. Plant Cell Environ. *20*, 713–721.

Cowtan, K. (2006). The Buccaneer software for automated model building. 1. Tracing protein chains. Acta Crystallogr. D Biol. Crystallogr. *62*, 1002–1011.

Davis, S.J., Vener, A.V., and Vierstra, R.D. (1999). Bacteriophytochromes: phytochrome-like photoreceptors from nonphotosynthetic eubacteria. Science *286*, 2517–2520.

Emsley, P., and Cowtan, K. (2004). Coot: model-building tools for molecular graphics. Acta Crystallogr. D Biol. Crystallogr. *60*, 2126–2132.

Essen, L.O., Mailliet, J., and Hughes, J. (2008). The structure of a complete phytochrome sensory module in the Pr ground state. Proc. Natl. Acad. Sci. USA *105*, 14709–14714.

Evans, K., Fordham-Skelton, A.P., Mistry, H., Reynolds, C.D., Lawless, A.M., and Papiz, M.Z. (2005). A bacteriophytochrome regulates the synthesis of LH4 complexes in Rhodopseudomonas palustris. Photosynth. Res. *85*, 169–180.

Giraud, E., and Verméglio, A. (2008). Bacteriophytochromes in anoxygenic photosynthetic bacteria. Photosynth. Res. *97*, 141–153.

Giraud, E., Fardoux, J., Fourrier, N., Hannibal, L., Genty, B., Bouyer, P., Dreyfus, B., and Verméglio, A. (2002). Bacteriophytochrome controls photosystem synthesis in anoxygenic bacteria. Nature *417*, 202–205.

Hughes, J., Lamparter, T., Mittmann, F., Hartmann, E., Gärtner, W., Wilde, A., and Börner, T. (1997). A prokaryotic phytochrome. Nature *386*, 663.

Kabsch, W. (2010). XDS. Acta Crystallogr. D Biol. Crystallogr. *66*, 125–132.

Kim, C.A., Gingery, M., Pilpa, R.M., and Bowie, J.U. (2002). The SAM domain of polyhomeotic forms a helical polymer. Nat. Struct. Biol. *9*, 453–457.

King, H.A., Hoelz, A., Crane, B.R., and Young, M.W. (2011). Structure of an enclosed dimer formed by the Drosophila period protein. J. Mol. Biol. *413*, 561–572.

Krissinel, E., and Henrick, K. (2007). Inference of macromolecular assemblies from crystalline state. J. Mol. Biol. *372*, 774–797.

Kyndt, J.A., Fitch, J.C., Meyer, T.E., and Cusanovich, M.A. (2005). Thermochromatium tepidum photoactive yellow protein/bacteriophytochrome/diguanylate cyclase: characterization of the PYP domain. Biochemistry *44*, 4755–4764.

Lamparter, T., Michael, N., Mittmann, F., and Esteban, B. (2002). Phytochrome from Agrobacterium tumefaciens has unusual spectral properties and reveals an N-terminal chromophore attachment site. Proc. Natl. Acad. Sci. USA *99*, 11628–11633.

Laskowski, R.A., MacArthur, M.W., Moss, D.S., and Thornton, J.M. (1993). PROCHECK: a program to check the stereochemical quality of protein structures. J. Appl. Cryst. *26*, 283–291.

Li, H., Zhang, J., Vierstra, R.D., and Li, H. (2010). Quaternary organization of a phytochrome dimer as revealed by cryoelectron microscopy. Proc. Natl. Acad. Sci. USA *107*, 10872–10877.

Marina, A., Waldburger, C.D., and Hendrickson, W.A. (2005). Structure of the entire cytoplasmic portion of a sensor histidine-kinase protein. EMBO J. *24*, 4247–4259.

Masuda, S., and Bauer, C.E. (2002). AppA is a blue light photoreceptor that antirepresses photosynthesis gene expression in Rhodobacter sphaeroides. Cell *110*, 613–623.

Masuda, S., Dong, C., Swem, D., Setterdahl, A.T., Knaff, D.B., and Bauer, C.E. (2002). Repression of photosynthesis gene expression by formation of a disulfide bond in CrtJ. Proc. Natl. Acad. Sci. USA *99*, 7078–7083.

Mosca, R., and Schneider, T.R. (2008). RAPIDO: a web server for the alignment of protein structures in the presence of conformational changes. Nucleic Acids Res. *36* (Web Server issue), W42–6.

Murshudov, G.N., Skubák, P., Lebedev, A.A., Pannu, N.S., Steiner, R.A., Nicholls, R.A., Winn, M.D., Long, F., and Vagin, A.A. (2011). REFMAC5 for the refinement of macromolecular crystal structures. Acta Crystallogr. D Biol. Crystallogr. *67*, 355–367.

Ritchie, D.W., Kozakov, D., and Vajda, S. (2008). Accelerating and focusing protein-protein docking correlations using multi-dimensional rotational FFT generating functions. Bioinformatics *24*, 1865–1873.

Rottwinkel, G., Oberpichler, I., and Lamparter, T. (2010). Bathy phytochromes in rhizobial soil bacteria. J. Bacteriol. *192*, 5124–5133.

Sali, A., and Blundell, T.L. (1993). Comparative protein modelling by satisfaction of spatial restraints. J. Mol. Biol. *234*, 779–815.

Schneider, T.R., and Sheldrick, G.M. (2002). Substructure solution with SHELXD. Acta Crystallogr. D Biol. Crystallogr. *58*, 1772–1779.

Söding, J. (2005). Protein homology detection by HMM-HMM comparison. Bioinformatics *21*, 951–960.

Tarutina, M., Ryjenkov, D.A., and Gomelsky, M. (2006). An unorthodox bacteriophytochrome from Rhodobacter sphaeroides involved in turnover of the second messenger c-di-GMP. J. Biol. Chem. *281*, 34751–34758.

Taylor, B.L., and Zhulin, I.B. (1999). PAS domains: internal sensors of oxygen, redox potential, and light. Microbiol. Mol. Biol. Rev. *63*, 479–506.

Ulijasz, A.T., Cornilescu, G., Cornilescu, C.C., Zhang, J., Rivera, M., Markley, J.L., and Vierstra, R.D. (2010). Structural basis for the photoconversion of a phytochrome to the activated Pfr form. Nature *463*, 250–254.

Vonrhein, C., Blanc, E., Roversi, P., and Bricogne, G. (2007). Automated structure solution with autoSHARP. Methods Mol. Biol. *364*, 215–230.

Wagner, J.R., Zhang, J., von Stetten, D., Günther, M., Murgida, D.H., Mroginski, M.A., Walker, J.M., Forest, K.T., Hildebrandt, P., and Vierstra, R.D. (2008). Mutational analysis of Deinococcus radiodurans bacteriophytochrome reveals key amino acids necessary for the photochromicity and proton exchange cycle of phytochromes. J. Biol. Chem. *283*, 12212–12226.

Wagner, J.R., Brunzelle, J.S., Forest, K.T., and Vierstra, R.D. (2005). A light-sensing knot revealed by the structure of the chromophore-binding domain of phytochrome. Nature *438*, 325–331.

Wagner, J.R., Zhang, J., Brunzelle, J.S., Vierstra, R.D., and Forest, K.T. (2007). High resolution structure of Deinococcus bacteriophytochrome yields new insights into phytochrome architecture and evolution. J. Biol. Chem. *282*, 12298–12309.

Winn, M.D., Ballard, C.C., Cowtan, K.D., Dodson, E.J., Emsley, P., Evans, P.R., Keegan, R.M., Krissinel, E.B., Leslie, A.G., McCoy, A., et al. (2011). Overview of the CCP4 suite and current developments. Acta Crystallogr. D Biol. Crystallogr. *67*, 235–242.

Yamada, S., Sugimoto, H., Kobayashi, M., Ohno, A., Nakamura, H., and Shiro, Y. (2009). Structure of PAS-linked histidine kinase and the response regulator complex. Structure *17*, 1333–1344.

Yang, X., Stojkovic, E.A., Kuk, J., and Moffat, K. (2007). Crystal structure of the chromophore binding domain of an unusual bacteriophytochrome, RpBphP3, reveals residues that modulate photoconversion. Proc. Natl. Acad. Sci. USA *104*, 12571–12576.

Yang, X., Kuk, J., and Moffat, K. (2008). Crystal structure of Pseudomonas aeruginosa bacteriophytochrome: photoconversion and signal transduction. Proc. Natl. Acad. Sci. USA *105*, 14715–14720.

Yang, X., Kuk, J., and Moffat, K. (2009). Conformational differences between the Pfr and Pr states in Pseudomonas aeruginosa bacteriophytochrome. Proc. Natl. Acad. Sci. USA *106*, 15639–15644.

Yang, X., Ren, Z., Kuk, J., and Moffat, K. (2011). Temperature-scan cryocrystallography reveals reaction intermediates in bacteriophytochrome. Nature *479*, 428–432.

